PERGAMON

Scripta Materialia 46 (2002) 753–757

Scripta MATERIALIA

www.actamat-journals.com

Kinetics of ferrite to austenite transformation during welding of 1005 steel

W. Zhang [a], J.W. Elmer [b], T. DebRoy [a,*]

[a] *Department of Materials Science and Engineering, The Pennsylvania State University, 212 Steidle Building, University Park, PA 16802-5005, USA*

[b] *Department of Chemistry and Materials Science, Lawrence Livermore National Laboratory, Livermore, CA 94551, USA*

Received 16 November 2001; received in revised form 25 January 2002; accepted 30 January 2002

Abstract

The kinetics of ferrite to austenite phase transformation in 1005 steel during welding was quantitatively determined by a combination of phase mapping using X-ray diffraction and transport phenomena based numerical modeling. The results can be used to calculate the phase transformation rates under various thermal cycles for this steel. © 2002 Published by Elsevier Science Ltd. on behalf of Acta Materialia Inc.

Keywords: Phase transformations; Steels; Kinetics; X-ray diffraction; Welding

1. Introduction

Understanding the evolution of weldment microstructure has been an important goal in contemporary welding research since the microstructure affects weldment properties. The main task to achieve this goal is to develop quantitative understanding of various phase transformation kinetics under rapid heating and cooling conditions during welding of important alloys. Post-weld microstructural characterization provides no information about either how the final structure is attained or at what rate various phase transformations take place during heating or cooling. The use of conventional experimental methods to study phase transformation kinetics such as dilatometry [1] under realistic welding conditions is inherently difficult. First, the conventional methods are indirect in that they measure certain changes in the welded sample (e.g. change in length) and cannot directly determine the amount of phases present during the test. Second, these methods cannot resolve the spatial distribution of phases encountered during welding [2]. Because of these problems, progress in this field has been slow and quantitative kinetic data pertaining to phase transformations in important alloy systems under the conditions of welding still remain scarce.

Much of the previous research on understanding weldment structure have focused on the microstructural studies of weld cross-sections to determine post-weld phase composition. During welding, microstructures that form during heating are subsequently altered by the transformations that take place during cooling. Therefore, what the

* Corresponding author. Tel.: +1-814-865-1974; fax:+1-814-865-2917.

E-mail address: debroy@psu.edu (T. DebRoy).

1359-6462/02/$ - see front matter © 2002 Published by Elsevier Science Ltd. on behalf of Acta Materialia Inc.
PII: S1359-6462(02)00040-4

traditional characterization of weldments really provides is a snapshot of the very last stage of a series of phase transformations that culminate in the eventual microstructure of the weldments.

A recently developed spatially resolved X-ray diffraction (SRXRD) technique can provide real time phase mapping of the weldment surface during welding. For example, during welding of steels, partial and complete transformations to α-ferrite, γ-austenite, and δ-ferrite phase regions have been identified using this technique with sufficient spatial resolution to identify the location of these phase fields at both low [2,3] and high heating and cooling rates [4]. However, analysis of the data collected by this newly developed technique to obtain phase transformation kinetics requires the knowledge of thermal cycles at various locations in the weldment. Measurement of temperature profiles in the weldment still remains a major challenge today. For the experiments reported in this paper, temperature measurements in the weldment would require placement of thermocouples at 0.25 mm intervals. Furthermore, X-ray measurements cannot be done where the thermocouples are placed. Hence, a practical recourse is to use a well-tested three-dimensional (3D) numerical heat transfer and fluid flow model to obtain accurate transient temperature fields, peak temperatures and heating and cooling rates at all locations of the weldment [5–7].

By combining the results of phase mapping work with transport phenomena based modeling, kinetics of important phase transformations can be quantitatively determined. This principle was demonstrated in a previous paper [8] that was focused on the kinetics of $\alpha \rightarrow \beta$ allotropic transformation during welding of commercially pure titanium. The kinetics of the transformation during continuous heating were quantitatively expressed using a modified Johnson–Mehl–Avrami (JMA) equation. In this paper, we select a more familiar and relatively straightforward example of $\alpha \rightarrow \gamma$ transformation during heating in the HAZ of plain carbon 1005 steel during gas tungsten arc (GTA) welding. The principle and the procedure to obtain quantitative kinetic data of $\alpha \rightarrow \gamma$ transformation with the initial results have been reported elsewhere [9]. Here we report and analyze new data on the kinetics of $\alpha \rightarrow \gamma$ transformation and, because of fairly large volume of the data, recommend a reliable quantitative rate equation for this phase transformation.

2. Procedure

The phase mapping work was done at the Stanford Synchrotron Radiation Laboratory [3]. The 1005 steel bar (0.05C, 0.31Mn, 0.18Si, 0.11Ni and 0.10Cr by wt.%) of 10.8 cm diameter was GTA welded at 1.9 kW power and 0.6 mm/s welding speed. The surface of the weldment was irradiated with an X-ray probe with high spatial resolution and the diffracted beam was collected to determine spatial variation of crystal structure. The results were then used to construct a phase map in various regions of the weldment top surface. The spatial distribution of the regions consisting of α, γ and δ phases, and the boundaries between these regions were qualitatively identified in the previous experimental work [3]. A portion of these data was further analyzed here using diffraction peak fitting routines to determine the peak area in each of the experimental SRXRD patterns [10]. This analysis was used to provide a semi-quantitative measure of the relative fractions of α and γ during the $\alpha \rightarrow \gamma$ transformation, which could then be modeled to extract additional kinetic information about this phase transformation.

The kinetic modeling approach used here assumes that the $\alpha \rightarrow \gamma$ transformation on heating involves nucleation and growth of γ phase, and that the rate of the transformation can be expressed by the following non-isothermal JMA equation [9,11]:

$$f = 1 - \exp\left[-\left\{ \sum_{i=1}^{m} k_0 \exp\left(-\frac{Q}{RT_i} \right) \Delta t \right\}^n \right] \qquad (1)$$

where f stands for the transformed γ phase fraction after time $m\Delta t$; Q, the activation energy of the $\alpha \rightarrow \gamma$ transformation involving nucleation and growth of γ phase; n, the JMA exponent; k_0, the pre-exponential constant; R, the universal gas constant; Δt, the time step; T_i, the temperature at ith time step; and m indicates the total number of

discrete time steps. A Q value of 117.07 kJ/mol for $\alpha \rightarrow \gamma$ transformation in steels that have similar compositions (0.08C, 0.45Mn, 0.03Si, 0.045S and 0.04P by wt.%) [12] as the 1005 steel was used in the present investigation. It should be recognized that the value of Q embodies both the driving force as well as the mobility terms and should be interpreted carefully. The values of k_0 and n need to be determined to quantitatively describe the kinetics of this transformation. For this purpose, Eq. (1) is linearized as follows:

$$\ln\{-\ln(1-f)\} = n\ln s + n\ln k_0 \tag{2}$$

where the symbol s is expressed as:

$$s = \sum_{i=1}^{m} \Delta t \exp\left(-\frac{Q}{RT_i}\right) \tag{3}$$

Eq. (2) indicates that the values of n and k_0 can be obtained from the slope and the intercept of a plot of $\ln\{-\ln(1-f)\}$ versus $\ln s$.

3. Results and discussion

Fig. 1 shows the spatial distribution of phases on one-half of the weldment top surface, since the weld is symmetrical about $y = 0$ plane. The stationary welding electrode is positioned at $x = y = 0$ while the welded sample moves from left to right along the x direction. Five phase regions were identified in Fig. 1: α single-phase region, $(\alpha + \gamma)$ two-phase region, γ single-phase region, $(\alpha + \gamma)$ two-phase region and liquid region [3]. The semi-quantitative data from the SRXRD peak area analysis showing the γ phase fractions along several monitoring lines perpendicular to the weld centerline were determined from the phase map and are summarized in Table 1 for the heating portion of the 1005 steel weld.

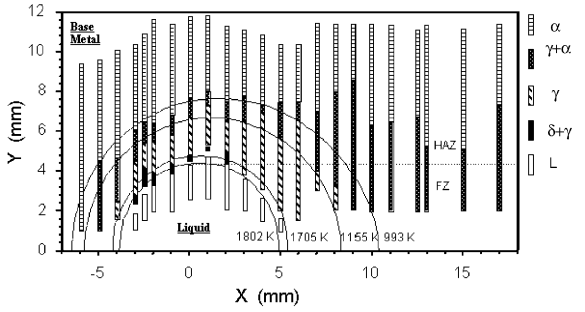

Fig. 1. Real-time SRXRD phase map of a 1005 steel arc weld. The superimposed isotherms were calculated from the 3D heat transfer and fluid flow model [9].

The calculation of s in Eq. (3) requires the knowledge of thermal cycles, which were computed using the 3D heat transfer and fluid flow model [9]. For each location indicated in Table 1, the value of s was calculated using Eq. (3) by summing the exponential term in Eq. (3) along the unique time–temperature path for each data point. The series of computed thermal cycles that were used for the calculations for various y locations leading to the $x = -3.0$ mm line are shown in Fig. 2. This summation was initiated at the A1

Table 1
Phase fractions of γ measured from the SRXRD phase map along various monitoring lines perpendicular to the weld centerline

$X = -5.0$ mm		$X = -3.5$ mm		$X = -3.0$ mm		$X = -2.5$ mm		$X = 0.0$ mm	
Y (mm)	γ Fraction	Y (mm)	γ Fraction	Y (mm)	γ Fraction	Y (mm)	γ Fraction	Y (mm)	γ Fraction
1.00	0.68	3.50	0.98	5.00	0.81	5.25	0.90	6.50	0.88
1.25	0.76	3.75	0.96	5.25	0.27	5.50	0.76	6.75	0.39
1.50	0.59	4.00	0.80	5.50	0.12	5.75	0.28	7.00	0.21
1.75	0.65	4.25	0.56	5.75	0.04	6.00	0.13	7.25	0.09
2.00	0.59	4.50	0.33			6.25	0.05		
2.25	0.38	4.75	0.13			6.50	0.01		
2.50	0.36	5.00	0.06						
2.75	0.17	5.25	0.02						
3.00	0.11								
3.25	0.05								
3.50	0.02								
3.75	0.01								

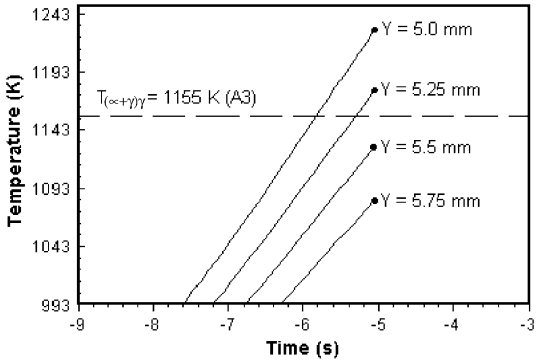

Fig. 2. Calculated thermal cycles at different locations along $x = -3.0$ mm line.

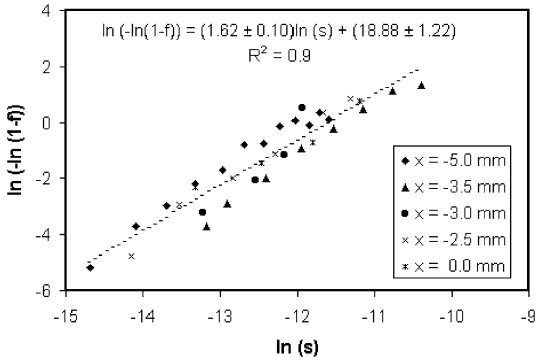

Fig. 3. The linearized JMA plot used to extract the JMA kinetic parameters.

temperature (993 K) since no $\alpha \rightarrow \gamma$ transformation takes place below this temperature [3], and ended at the maximum temperature experienced by each data point as indicated by the solid circles in Fig. 2.

The results of these calculations are plotted in Fig. 3 as the linearized JMA data of $\ln\{-\ln(1-f)\}$ versus $\ln s$. The values of the slope and the intercept of the plot were determined from a linear regression analysis to yield the kinetic parameters n and $\ln(k_0)$. The results showed that the values of n and $\ln(k_0)$ were 1.62 ± 0.10 and 11.63 ± 1.46, respectively. These values are consistent with those reported in our previous paper ($n = 1.9$ and $\ln(k_0) = 11.80$) [9] where only SRXRD data leading to the $x = -2.5$ mm line were used. It should be noted that the value of n has significantly less

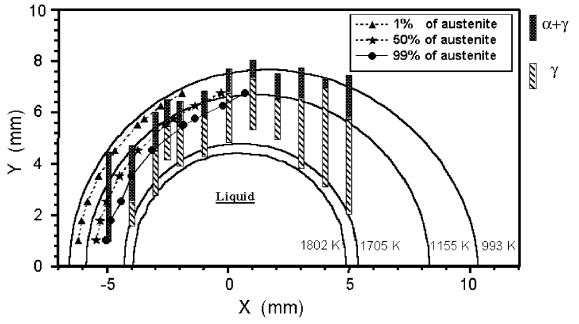

Fig. 4. Comparison between the calculated and experimental $\alpha/(\alpha+\gamma)$ and $(\alpha+\gamma)/\gamma$ boundaries. The extent of $\alpha \rightarrow \gamma$ transformation was calculated by a combination of the modified JMA equation and the computed thermal cycles.

uncertainty than the value of k_0. This is because the value of n is directly obtained from the slope of the plot in Fig. 3 whereas the value of k_0 requires an exponential function that magnifies the uncertainty in the value of k_0.

In order to check the internal consistency of the SRXRD data and the JMA kinetic parameters, the parameters obtained from Fig. 3 and the calculated thermal cycles were used in Eq. (1) to reconstruct the locations where the calculated phase fraction of γ is equal to 1%, 50%, and 99%. These locations are shown in Fig. 4. In this figure, it is assumed that the 1% and 99% of γ represents the start and end of the transformation, respectively. Hence the 1% and 99% of γ profiles represent the calculated $\alpha/(\alpha+\gamma)$ and $(\alpha+\gamma)/\gamma$ spatial boundaries, respectively. The experimental $\alpha/(\alpha+\gamma)$ and $(\alpha+\gamma)/\gamma$ spatial boundaries correspond to the top ends of $(\alpha+\gamma)$ and γ bars, respectively. As shown in Fig. 4, the calculated $\alpha/(\alpha+\gamma)$ and $(\alpha+\gamma)/\gamma$ spatial boundaries agree well with those determined from the SRXRD phase map. Thus, the computed JMA kinetic parameters are consistent with the phase map.

Apart from providing a quantitative basis for the calculation of $\alpha \rightarrow \gamma$ transformation kinetics, the values of the kinetic parameters also provide insight about the transformation mechanism. For diffusion-controlled growth, the value of JMA exponent, $n = 1.6$, is consistent with a phase transformation mechanism whereby γ nucleates and grows from the α matrix with a nucleation rate

that decreases with time [13]. This mechanism can be rationalized by considering the existence of ferrite/cementite interfaces within the pearlite colonies in the starting microstructure that provide preferred nucleation sites for γ phase. After these sites are exhausted, other sites, such as α grain boundaries and secondary particles, may still be active for further nucleation of γ. However, the nucleation rates at these sites may be lower than those within the pearlite colonies.

It should be noted that the two JMA kinetic parameters, k_0 and n, depend on the initial microstructure of the base metal. However, this dependence cannot be determined at this time in view of the scarcity of kinetic data in the literature. The lack of available data emphasizes the need for quantitative investigations on this topic and suggests that the parameter values obtained in this investigation should be used carefully.

4. Summary and conclusions

In summary, the $\alpha \rightarrow \gamma$ transformation during heating in 1005 steel arc welds was studied experimentally by the SRXRD technique and modeled using a combination of a 3D heat transfer and fluid flow model and a non-isothermal JMA equation. The JMA kinetic parameters for the transformation were determined from the kinetic data obtained by the SRXRD technique. The kinetics of $\alpha \rightarrow \gamma$ transformation could be satisfactorily predicted using the JMA equation and the calculated thermal cycles. Furthermore, the JMA exponent of 1.6 is consistent with the fact that during the $\alpha \rightarrow \gamma$ phase transformation in 1005 steel, the nucleation rate of γ phase from α matrix decreases with time. The research reported in this paper represents a contribution to the growing quantitative knowledge base in welding. Expansion of this knowledge base is necessary, if not essential, to achieve structurally sound, defect free welds based on scientific principles.

Acknowledgements

Mr. Wei Zhang gratefully acknowledges support from a Fellowship from the American Welding Society. The work at Penn State was also supported by a grant from the US Department of Energy, Office of Basic Energy Sciences, Division of Materials Sciences, under grant number DE-FGO2-01ER45900. The LLNL portion of this research was performed under the auspices of the US Department of Energy, Lawrence Livermore National Laboratory, under contract no. W-7405-ENG-48. The authors thank Todd A. Palmer and Brandon Wood of LLNL for their assistance with the analysis of X-ray diffraction data.

References

[1] Valentich JH. Tube type dilatometers: applications from cryogenic to elevated temperatures. Research Triangle Park: Instrument Society of America; 1981.
[2] Elmer JW, Wong J, Fröba M, Waide PA, Larson EM. Metall Mater Trans 1996;27A:775.
[3] Elmer JW, Wong J, Ressler T. Metall Mater Trans 2001;32A:1175.
[4] Elmer JW, Wong J, Ressler T. Scripta Mater 2000;43:751.
[5] Mundra K, DebRoy T, Kelkar K. Numer Heat Transfer 1996;29:115.
[6] Pitscheneder W, DebRoy T, Mundra K, Ebner R. Welding J 1996;75:71s.
[7] Yang Z, DebRoy T. Metall Mater Trans 1999;30B:483.
[8] Yang Z, Elmer JW, Wong J, DebRoy T. Welding J 2000;79:97s.
[9] Zhang W, Elmer JW, DebRoy T. Mater Sci Eng A, in press.
[10] Lawrence Livermore National Laboratory, July, 2001, unpublished results.
[11] Kruger P. J Phys Chem Solids 1993;54:1549.
[12] Nath SK, Ray S, Mathur VNS. ISIJ Int 1994;34:191.
[13] Christian JW. The theory of transformations in metals and alloys. 2nd ed. Part I Oxford: Pergamon; 1975.